

## CFD SIMULATION OF TRUSS SPAR VORTEX-INDUCED MOTION

Sampath Atluri  
Technip USA, Houston, Texas

John Halkyard  
Technip USA, Houston, Texas

Senu Sirnivas  
Technip USA, Houston, Texas

### ABSTRACT

Helical strakes are used to suppress the Vortex-Induced Motion of Truss Spars. Model experiments have demonstrated the efficiency of strakes in the Truss Spar design but also indicate that the VIM response is sensitive to the details of strake design and placement of appurtenances around the Spar hull. It is desirable to study these hydrodynamic effects using CFD. The following paper is a continuation of some of the earlier CFD simulations on this subject (see, J. Halkyard, et al., "Benchmarking of Truss Spar Vortex-Induced Motions Derived from CFD with Experiments", Proceedings of OMAE'05). This paper in particular deals with the effect of holes in the strakes and appurtenances and their placement. All the simulations were done at model scale (1:40 scale model of an actual Truss Spar design) to compare the motions with experimental results. Mesh sensitivity and turbulence modeling issues are also discussed. Calculations were done using general purpose CFD code Acusolve™.

### INTRODUCTION

Truss Spars are in operation in Gulf of Mexico for several years. A typical Truss Spar has a cylindrical hull floating vertically with an open truss section attached at the bottom as shown in Figure 1. The diameter of the Spar hull can vary from 70 to 150 ft. Detailed explanation about the design of Truss Spars can be obtained in [1]. Subjected to loop currents, these Spars undergo Vortex-Induced Motions (VIM). VIM is a result of oscillating surface pressure induced by alternate vortex shedding from either side of the structure. The motion in transverse direction to the flow is more predominant compared to that in the inline direction [2]. To mitigate VIM, helical strakes are used on all the spar hulls. These strakes are usually three-stranded and assumed to break the correlation of vortices in the span wise direction (along the length of the cylinder). More arguments on the physics of strake performance can be obtained in [3].



Figure 1: Typical Truss Spar

Rigorous experiments on scaled down spar models are frequently conducted to study their response. One such experiment series is documented in [4]. The model used was scaled at 1:40 (Froude scale) of an actual Truss Spar. The following paper is a continuation of earlier efforts [5] in simulating the VIM of this truss spar model using CFD techniques.

### NOMENCLATURE

|           |  |
|-----------|--|
| $\vec{u}$ | = Current velocity vector                      |
| $\vec{U}$ | = Relative velocity vector                     |
| $\vec{x}$ | = Spar velocity vector                         |
| $\rho$    | = density of water                             |
| $U_m$     | = Reduced velocity based on calm water period  |
| $T_n$     | = Natural period in calm water without current |
| $D$       | = Diameter                                     |

- L = Characteristic length of truss
- u = Current velocity magnitude
- $C_d$  = Drag coefficient
- $C_a$  = Added mass coefficient

**MODEL TESTS**

The experiment model is as shown in Figure 2. As in a full scale Spar, mooring chains run along the length of the hull and holes are made in the strakes to accommodate these chains. The tests are conducted by pulling the model and taking motion and drag measurement. Details of the experimental setup can be obtained from [4]. The model tests [4] were done for several current headings with different inflow current speeds. The operating Reynolds numbers were in the range of 70,000 to 200,000.



Figure 2: Photo of the model

Similar to the bare cylinder VIV literature, the non-dimensional parameters for a straked Spar can be based on the diameter of the hull  $D$  and the velocity of the flow  $U$ . Reduced velocity  $U_m$  can be given as

$$U_m = \frac{uT_n}{D}$$

For a given geometry, all the experiments can be classified based on the current heading (Hdg) and the reduced velocity ( $U_m$ ). The relative direction of current with respect to the

model can be seen in Figure 3. The effectiveness of helical strakes to mitigate VIM of Spar hulls is well demonstrated in the literature [4] [6]. However, the performance of the strakes is argued to be affected by the placement of appurtenances like mooring chains, fairleads etc., that run along the length of the hull (Figure 2). One of the objectives of this study is to verify the affect of these appurtenances using CFD. In the present work, the mooring chains are modeled as pipes running along the length of the hull and connected to the fairleads. The strakes have holes to accommodate the chains. The pitch of the strakes is  $4.5D$  and each strake covers exactly one third of the circumference. Width of the strake is 13% of the hull diameter.

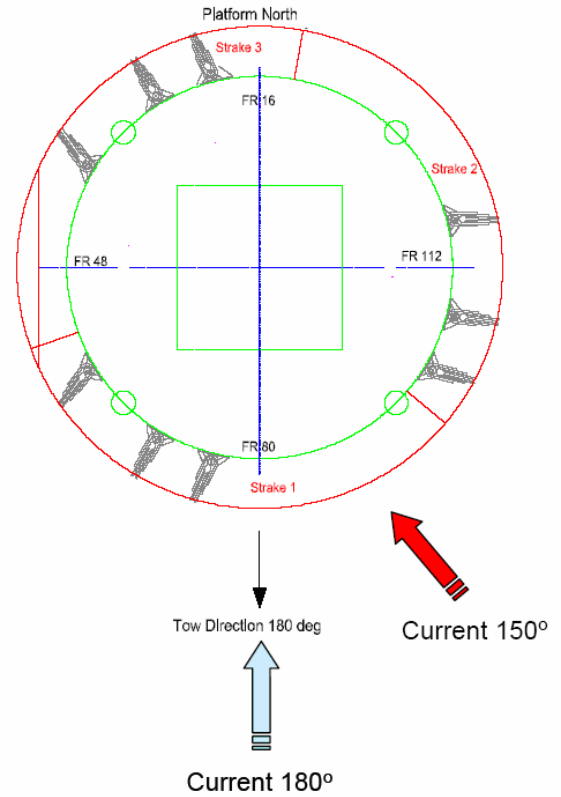


Figure 3: Flow direction layout

In the model tests, the mooring design allows the model to move in six degrees of freedom; surge, sway, heave, pitch, roll and yaw. However, the predominant motion was always in the transverse (sway) and in-line (surge) directions to the incoming flow and negligible in all other directions. Hence, our CFD model was allowed to move only in these two directions.

## CFD ANALYSIS

To improve mesh economy, the truss section of the spar was not modeled explicitly in the initial CFD calculations. Instead, the truss forces were calculated using Morison's equations, the details of which are included below. Recent calculations with explicit truss section model showed better results compared to using the Morison formulation. The 3D geometries for all the models used in the present work are shown in Figure 4. Model I and Model II differ by the inclusion of holes on strakes and appendage in the latter. Model III includes the truss section. It can be noted that Model I is similar to the geometry considered in earlier work [5] which used a hexahedral mesh. The mesh used in the present work is all tetrahedral and hence Model I is re-calculated for validation of the new mesh. For convenience, from here on, the mesh for Model I, Model II and Model III will be referred to as Mesh A, Mesh B and Mesh C respectively. Mesh sizes varied from approximately 200,000 nodes for Model I to 600,000 nodes for Model III. These meshes have a better near wall resolution compared to [5].

Finite Element CFD solver, Acusolve™, is used for all the calculations [7]. Acusolve™ is based on the Galerkin/Least Squares formulation and supports a variety of element types. Acusolve™ uses a fully coupled pressure/velocity iterative solver plus a generalized alpha method as a semi-discrete time stepping algorithm. Acusolve™ is second order accurate in space and time. Figure 5 shows the flow domain in general and Figure 6 compares the mesh without and with appurtenances (i.e., Mesh A and Mesh B respectively). The mesh is designed with small grid spacing near the cylinder and the near wake region, and relatively coarse grid spacing elsewhere in order to provide an economical grid. The top of the flow domain (free surface) corresponds to the top of the hull and is assigned with a fixed boundary condition as 'free slip'. A wall function was used to describe the flow adjacent to the surface of the spar which greatly economized the mesh. The average surface  $y^+$  was equal to 20. Turbulence was modeled using Spalart's Detached Eddy Simulation (DES) technique [8]. The DES is a hybrid model that combines the accuracy and economy of Spalart-Allmaras (SA) model [9] for attached boundary layers with the accuracy of LES (with Smagorinsky sub grid scale modeling) for separated eddies. The transition between the RANS and LES is smooth and all the constants used for the model are standard. The Morison forces on the truss section and the mooring system are modeled using a user function for models I and II. The Morison's equations to calculate hydrodynamic forces are

$$\bar{F} = \frac{1}{2} \rho C_d L^2 \bar{U} |\bar{U}| + \rho C_a L^3 \frac{\partial \bar{U}}{\partial t} \quad \text{and} \quad \bar{U} = \bar{u} - \bar{x}$$

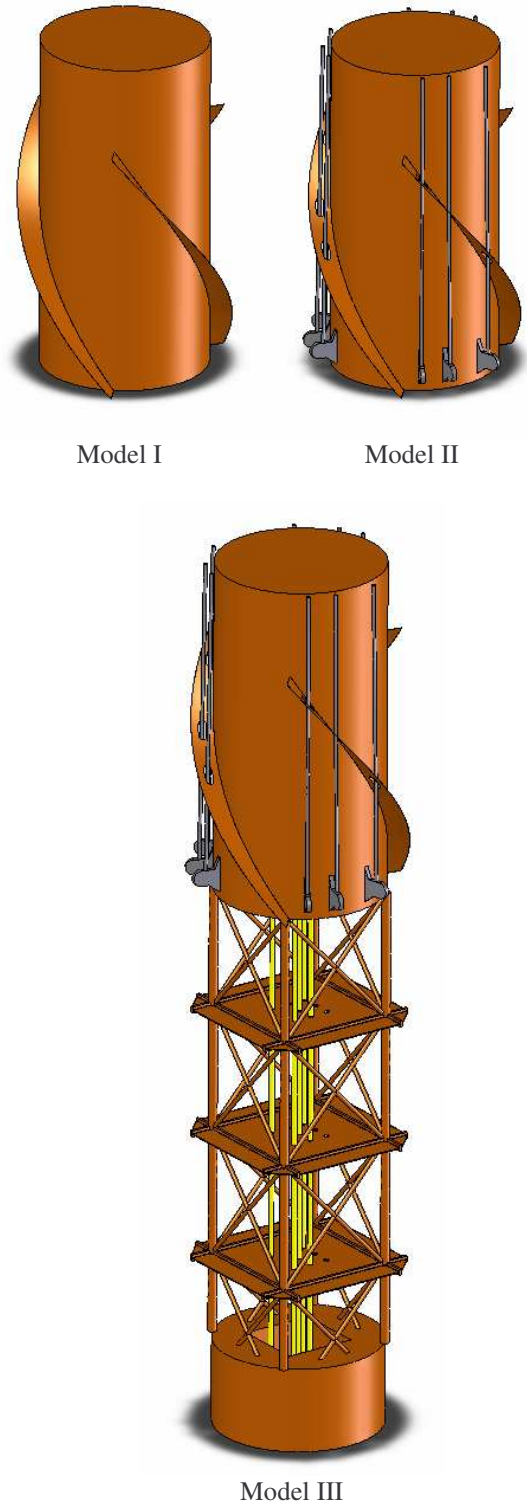


Figure 4: 3D geometry comparison

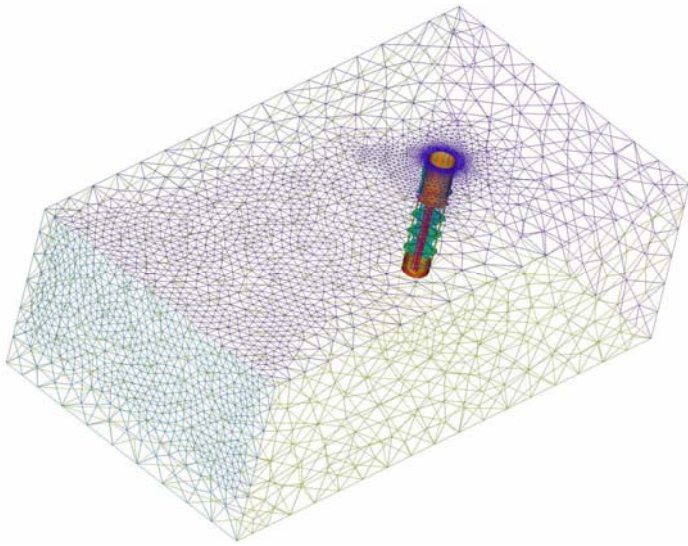


Figure 5: Flow domain

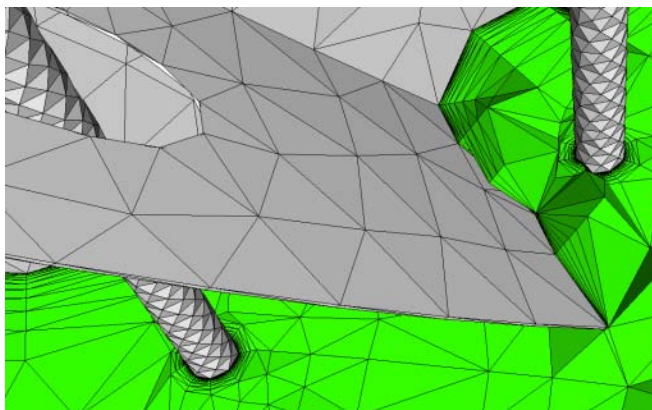
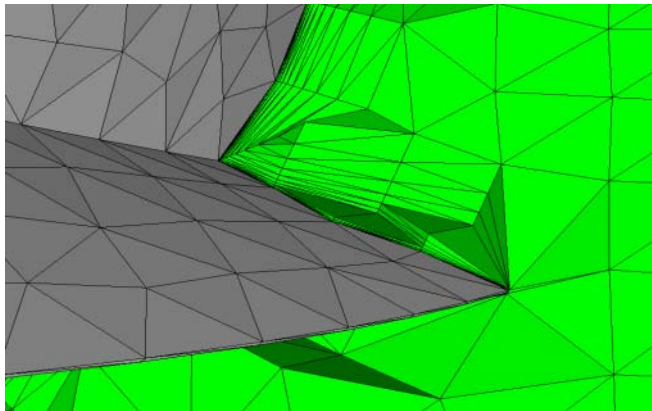


Figure 6: Mesh close up view (without and with appurtenances)

The force vector is calculated by assuming that the force on the truss arises from drag and added mass (acceleration) contributions. The drag contribution (the first term on the right

hand side) is determined by a drag coefficient, a characteristic length scale, and the spar velocity relative to the free stream velocity  $U$ . Note that the drag coefficient must include the projected area when multiplied by the characteristic length. The added mass term is formed in a similar manner. As implemented here, we did not account for the changes in the added mass and drag coefficients with the direction of mass or acceleration relative to the free stream flow although this could be done. The coefficients for truss and soft tank added mass and drag were derived from formulations for fixed jacket structures in API RP2A and from previous model test programs.

In the simulations, the motion of the spar is calculated within each time step by first determining the integral of the surface tractions on the hard tank from the CFD solution. This is provided by the AcuSolve flow solution. The forces due to the mooring system are calculated from the current spar position and forces on the truss are calculated from the current velocity and kinematics of the spar with respect to the free stream current. The new position of the spar for the next time step is found by a simple integration using the trapezoidal rule. In effect, the new position of the spar is calculated using the force values at the middle of the step.

The free body motion of the Spar within the mesh is accommodated using a specified mesh boundary condition. The location of each node is specified based on the position of the Spar at every time step. This approach avoids the solution of nodal locations using an arbitrary elastic solid to represent the mesh (Arbitrary Lagrangian Eulerian or ALE method) and hence solve for the new nodal locations. However, the fluid flow is calculated based on the new nodal locations as in the ALE method.

### **Mesh Convergence**

To test the mesh convergence, we considered a test case with current heading of 150 degrees and reduced velocity of 7. A typical Mesh A used for calculations reported here contained about 200,000 nodes. A fine mesh with 600,000 nodes (for the same model) with increased resolution near the hull surface and the wake was used for convergence test. Both the cases were run for at least 20 cycles of vibration and no significant difference in the statistics of response were observed.

### **Free Decay Test**

For the CFD model, free decay test was performed to verify the natural oscillation period of the system. The Spar is displaced to about  $0.3D$  in the transverse direction and allowed to oscillate freely in the absence of the flow. The mean zero crossing sway period was 25.5 seconds (Figure 7). The sway natural period of the system measured in the experiments was 25.3 seconds.

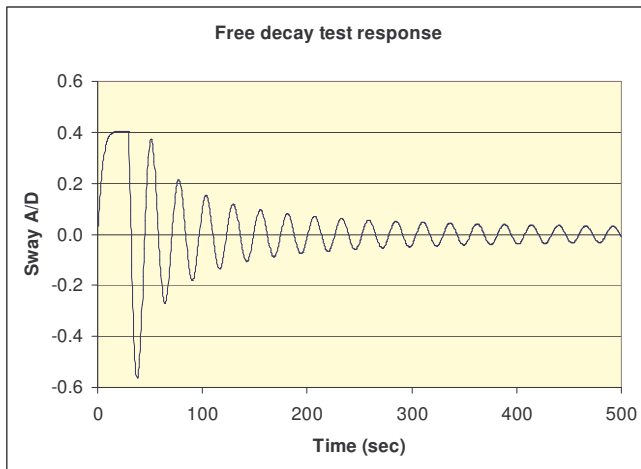


Figure 7: Free decay test;  $T_n = 25.5$  sec

All the calculations reported here were performed on a 32 CPU Linux cluster and typical run times for 1000 time steps (more than 20 oscillations) was observed to be about 2 hours for Mesh A (without appurtenances), 4 hours for Mesh B (with appurtenances) and 6 hours for Mesh C (with appurtenances and truss). The response comparisons mainly focus on Sway motion (transverse vibration) in the following discussion. Typically, the standard deviation and the average maximum response are of interest. The ‘average maximum’ response can be defined as the

$$\text{Max A/D} = (\text{Max Y/D} - \text{Min Y/D})/2$$

where, Y is the sway displacement.

## RESULTS AND DISCUSSION

Two series of tests were performed. The current heading was kept constant at 150 degrees for the first series and the inflow velocity was varied to achieve a reduced velocity range of 4 ~ 10. In the second series, the reduced velocity was kept constant at 7 and the current heading was varied. Results were compared for the three models. All the responses are presented as a ratio of the diameter of the cylinder. Figures 8 and 9 show the Sway standard deviation and ‘average maximum’ for models I, II and III in comparison with the experiment. In general, the standard deviation is a better measure for comparison rather than the ‘average maximum’ as the latter depends greatly on the time length of simulation. From Figure 8, Model I response is similar to earlier results [5] thus validating the new tetrahedral mesh. The response of Model II is higher than that of Model I for certain flow velocities suggesting that appurtenances may or may not influence the VIV response. However, CFD calculations over predicted the response for both these models. When the truss section is explicitly modeled in Model III without using the Morison formulation, the response showed very good agreement with

the experiment. The agreement is reasonably good in Figure 9 for ‘average maximum’ response. The second series of tests is ongoing work and only preliminary results are presented. Figures 10 and 11 show response sensitivity with respect to current heading. CFD response is over predicted compared to experiments for models I and II. Model III shows good agreement with experiments for most of the low response cases. The reason for anomalies, (for example, current heading 180 @  $U_{rn} \sim 7$ ), is yet to be explained. However, the overall trends are encouraging.

Figure 12 shows the time series of sway and surge vs. sway plots for a high response case (current heading 150 degrees and  $U_{rn} \sim 10$ ). The classic ‘8’ shape can be noticed in the experiment but not as evident in the CFD simulation (Model III was considered here). Also, the sway time series from the experiment shows some modulation where as the sway from CFD does not. Figure 13 shows similar plots for a low response case (current heading 150 degrees and  $U_{rn} \sim 4$ ). Here, the motion is small in both the cases and there are no distinctive patterns in surge or sway.

## CONCLUSION

CFD calculations show some effect of including the appurtenances. The response was either higher or remained the same with the addition of appurtenances. But the difference in response is small especially when compared to the experimental results. Hence, modeling the appurtenances in CFD may be avoided to gain speed in the calculations. However, this observation requires further validation by performing experiments with and without appurtenances and considering several test cases in CFD. Also, these observations are valid for models that did not include the truss section explicitly. Modeling the truss section along with the hull made a huge improvement in the response statistics. Hence, explicit modeling of the truss section may be important. On the contrary, the computing time suffers due to increase in mesh size if the truss is explicitly modeled. Hence, it is desired to improve the Morison formulation for the truss section and work is in progress in this direction. In general, the response trends are good and hence similar analysis can be readily used to study flow pattern and aid design of VIV mitigation devices before going into an extensive model test program.

## ACKNOWLEDGEMENTS

The authors would like to thank Technip for permission to publish these findings.

## REFERENCES

- [1] Bangs, A. S., Miettinen, J. A., Mikkola, T. P. J., Silvola, I., and Beattie, S. M., 2002, "Design of the Truss Spars for the Nansen/Boomvang Field Development," Proceedings Offshore Technology Conference, Houston, Texas, Paper Number OTC 14090.
- [2] Blevins R.D., 1990, Flow-Induced Vibration, Van Nostrand Reinhold, New York.
- [3] Bearman, Peter and Brankovic, Maša., 2002, "Passive Control of Vortex Induced Vibration", Proceedings Conference on Bluff Body Wakes and Vortex-Induced Vibrations (BBVIV3), Port Douglas, Australia.
- [4] Irani, Mehernosh and Finn, Lyle., 2005, "Improved Strake Design for Vortex Induced Motions of Spar Platforms", Proceedings 24th International Conference on Offshore Mechanics and Arctic Engineering, OMAE'05-67384, Halkidiki, Greece.
- [5] Halkyard, J., Sirmivas, S., Holmes, S., Constantinides, Y., Oakley, O. and Thiagarajan, K., 2005, "Benchmarking of Truss Spar Vortex Induced Motions Derived from CFD with Experiments", OMAE 2005-67252, Halkidiki, Greece.
- [6] Irani, Mehernosh and Finn, Lyle, 2004, "Model Testing for Vortex Induced Motions of Spar Platforms", Proceedings 23rd International Conference on Offshore Mechanics and Arctic Engineering, OMAE'04-51315, Vancouver, B.C., Canada.
- [7] www.acusim.com
- [8] Travin A., Shur M., Strelets M., Spalart P.R., 2000, "Detached-Eddy Simulations past a Circular Cylinder", Flow, Turb. Comb., 63, pp. 293-313.
- [9] Spalart, P. R. and S. R. Allmaras., 1992, "A one-equation model for aerodynamic flows," AIAA 92-0439.

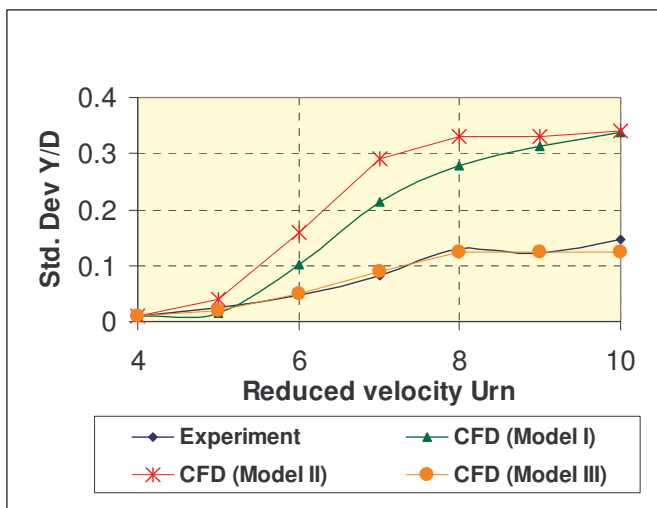


Figure 8: Response (Std. Dev) at current heading 150 deg

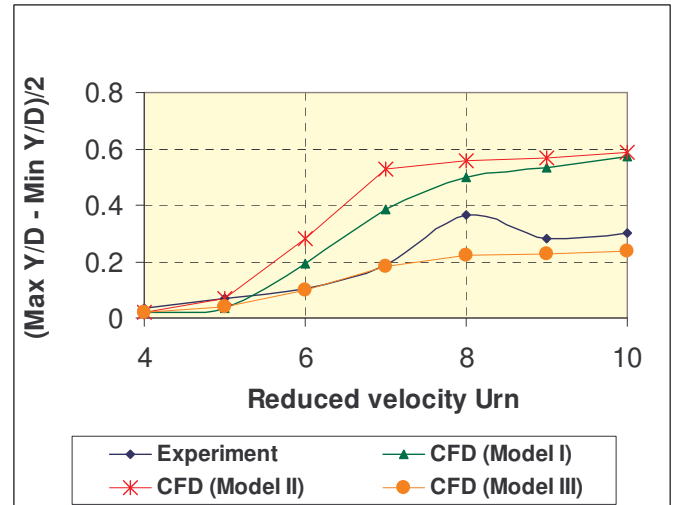


Figure 9: Response ('average maximum') at current heading 150 deg

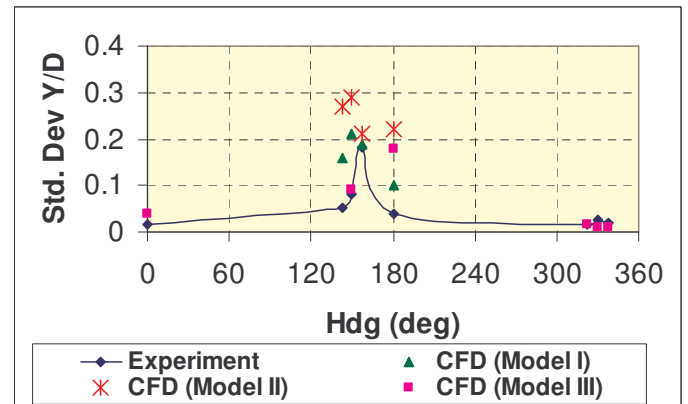


Figure 10: Response (Std. Dev) at Urn ~ 7

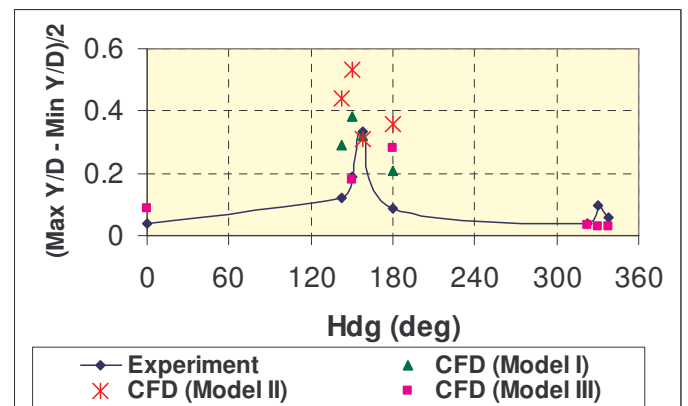


Figure 11: Response ('average maximum') at Urn ~ 7

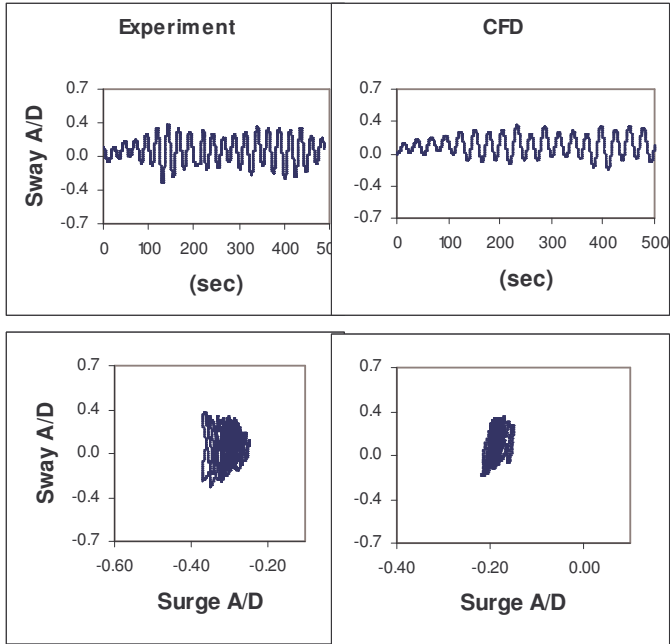


Figure 12: Response comparison current heading 150 deg;  
Urn ~ 10

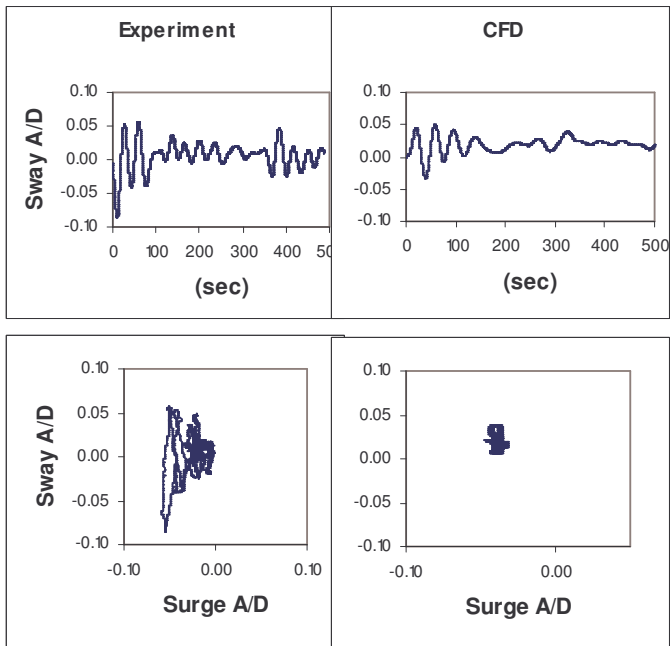


Figure 13: Response comparison current heading 150 deg;  
Urn ~ 4